

EVIDENCE OF INTERNAL DISSIPATION ORIGIN FOR THE HIGH-ENERGY PROMPT EMISSION OF GRB 170214A

QING-WEN TANG^{1,2,3}, XIANG-YU WANG^{4,5}, RUO-YU LIU⁶

¹Department of Physics, Nanchang University, Nanchang 330031, China

²Center for Cosmology and AstroParticle Physics (CCAPP), The Ohio State University, Columbus, OH 43210, USA

³Guangxi Key Laboratory for Relativistic Astrophysics, Nanning 530004, China

⁴School of Astronomy and Space Science, Nanjing University, Nanjing 210093, China

⁵Key Laboratory of Modern Astronomy and Astrophysics (Nanjing University), Ministry of Education, Nanjing 210093, China

and

⁶Max-Planck-Institut für Kernphysik, D-69117 Heidelberg, Germany

ABSTRACT

The origin of the prompt high-energy ($> 100\text{MeV}$) emission of gamma-ray Bursts (GRBs), detected by the Large Area Telescope (LAT) on board the *Fermi* Gamma-ray Space Telescope, for which both an external shock origin and internal dissipation origin have been suggested, is still under debate. In the internal dissipation scenario, the high-energy emission is expected to exhibit significant temporal variability, tracking the keV/MeV fast variable behavior. Here, we report a detailed analysis of the *Fermi* data of GRB 170214A, which is sufficiently bright in the high energies to enable a quantitative analysis of the correlation between high-energy emission and keV/MeV emission with high statistics. Our result shows a clear temporal correlation between high-energy and keV/MeV emission in the whole prompt emission phase as well as in two decomposed short time intervals. Such a correlation behavior is also found in some other bright LAT GRBs, e.g., GRB 080916C, 090902B and 090926A. For these GRBs as well as GRB 090510, we also find the rapid temporal variability in the high-energy emission. We thus conclude that the prompt high-energy emission in these bright LAT GRBs should be due to an internal origin.

Keywords: gamma-ray burst: individual (GRB 170214A) C radiation mechanisms: non-thermal

1. INTRODUCTION

Gamma-ray bursts (GRBs) are the most intense astrophysical explosions in the universe. The most popular model for interpreting the highly variable keV-MeV emission, such as internal shocks, is the internal dissipation model. In recent years, *Fermi* Large Area Telescope (LAT; 20 MeV to more than 300 GeV) has detected prompt and long-lived high-energy ($> 100\text{ MeV}$) gamma-ray emissions from a large number of GRBs, such as GRB 080916C, GRB 090510, GRB 090902B, GRB 090926A and GRB 130427A (Abdo et al. 2009a; Ackermann et al. 2010; Abdo et al. 2009b; Ackermann et al. 2011, 2014). The long-lived high-energy emissions are believed to be produced by the external shocks (Kumar & Barniol Duran 2009, 2010; Corsi et al. 2010; De Pasquale et al. 2010; Gao et al. 2009; Ghirlanda et al. 2010; Ghisellini et al. 2010; Wang et al. 2010; Razzaque 2010), via synchrotron emission and/or inverse-Compton processes. However, the origin of the high-energy photons during the prompt phase is still uncertain. It has been suggested that the prompt high-energy emission also arises from the external shocks, via synchrotron radiation (e.g., Kumar & Barniol Duran (2009)) or scattering prompt MeV photons by the accelerated electrons there (Beloborodov et al. 2014). Such external origin models predict a smooth light curve of high-energy emission. On the other hand, there have been indications of the internal origin of the prompt high-energy emissions for some GRBs, such as GRB 090926A and GRB 090902B, as prompt high-energy emissions show a variable structure correlating with the keV-MeV emission (Ackermann et al. 2011; Zhang et al. 2011). If such a temporal behavior of high-energy emission is real, it would favor

the internal origin scenario.

Recently, *Fermi*-LAT observed a bright GRB 170214A, with more than one hundred of > 100 MeV photons within the first 200 seconds, which makes it a good case for studying the temporal correlation in a statistical way. In this work, we present a quantitative analysis of the prompt variable keV-MeV and high-energy emissions of GRB 170214A, and compare it with other bright LAT GRBs.

2. DATA ANALYSIS

2.1. Properties of GRB 170214A

Fermi Gamma-Ray Burst Monitor (GBM, energy coverage of 8 keV-40 MeV) is triggered by GRB 170214A at $T_0 = 15:34:26.92$ UT on 14 February 2017 (T_0 , the GBM trigger time). The GBM light curve shows multiple overlapping peaks with a T_{90} duration of about 123 seconds (Mailyan & Meegan 2017). Simultaneously, *Fermi*-LAT detected high-energy emission from GRB 170214A, at a location of R.A. = 256.33, decl. = -1.88 (J2000) (Mazaeva et al. 2017), which is consistent with that detected by *Fermi*-GBM. More than 160 photons above 100 MeV, with 13 of them above 1 GeV, are observed within 1000 seconds (Mazaeva et al. 2017), which makes it a good case to perform time-resolved analysis of high-energy emission.

The Konus-Wind detected the multi-peak lightcurve with a T_{90} duration of about 150 seconds (Frederiks et al. 2017). *Swift*-XRT detected an afterglow emission close to the LAT position (Beardmore et al. 2017a,b). Follow-up observations in the optical and/or NIR band are performed by RATIR (the Reionization and Transients Infrared Camera), NOT (the Nordic Optical Telescope), GROND and Mondy (the AZT-33IK telescope in Sayan observatory) (Troja et al. 2017a,b; Malesani et al. 2017; Schady et al. 2017; Schady & Kruehler 2017; Mazaeva et al. 2017). The ESO Very Large Telescope detected a faint optical afterglow and claimed a redshift of $z = 2.53$ (Kruehler et al. 2017).

2.2. LAT data analysis

Within 12 degrees of the reported LAT position, R.A. = 256.33, decl. = -1.88 (J2000) (Mazaeva et al. 2017), the Pass 8 transient events are used in the energy range of 100 MeV to 10 GeV. These data are analyzed using the *Fermi* ScienceTools package (v10r0p5) available from the *Fermi* Science Support Center (FSSC)¹. Events with zenith angles $> 100^\circ$ are excluded to reduce the contribution of Earth-limb gamma rays. Instrument response function “P8R2_TRANSIENT020_V6” is used. GRB 170214A is modeled as a point source with the corresponding position and the photon spectrum is assumed to be a power law, i.e., $dN/dE = N_0(E/100\text{MeV})^{-\Gamma_{\text{LAT}}}$, with the normalization factor (N_0) and photon index (Γ_{LAT}) as free parameters. A background model comprises the galactic interstellar emission model (“gll_iem_v06.fits”) and extragalactic isotropic spectral template (“iso_P8R2_TRANSIENT020_V6_v06.txt”). For these diffuse components in the model, we calculate the response files by the *gtdiffresp* tool. The livetime cube and exposure maps are generated by the *gltcube* and *gtexpmap* tool. We run the *gtlike* tool to derive the best fit.

We first perform a blind search in three good time intervals, i.e., 0 – 900, 2500 – 7000 and 8500 – 13000 second after the GBM trigger. The strong emission exists in the first 900 seconds, after which no significant emission is found.

Second, 10 and 100 seconds are employed as the resolved time bin before and after $T_0 + 200$ seconds respectively, when performing the time-resolved analysis of the first 900 seconds data. The nearby time bin is combined if the error of the energy flux in one time bin is larger than then central value. For the intensive emission period, i.e., 52-70 s, we divide this time interval into 7 bins. Before 52 s, the LAT show a marginal significant emission, which is treated as a single time bin. The likelihood results, i.e., the photon flux (F_L) and energy flux (f_L) are present in Tab. 1, where the total photon number within 12 degrees (N_{ROI}), the predicted photon number (N_P) and the test-statistic value (TS, the square root of TS approximately equals to the detection significance (Mattox et al. 1996)), are also given.

2.3. GBM data analysis

Given the recommendation for selecting the detectors with high counts rate above background, the Time Tagged Event (TTE) data from two NaI detectors (n0, n1) and one BGO detector (b0) are taken from FSSC and analyzed with the software package RMFIT version 4.3pr2². We select the energy range of 8 – 1000 keV for two NaI detectors and of 200 keV–10 MeV for a BGO detector. A first order polynomial is applied for each detector to fit the background with flat counts rate regions pre- and post-burst.

We select the time bins same as that used in LAT analysis in the time interval of 52 – 160 s, after which there is no significant emission in GBM band. Before 52 s, we perform a small time bins, i.e., 2 seconds per time bin, since it is a fast variable (hereafter

¹ <https://fermi.gsfc.nasa.gov/ssc/>

² <https://fermi.gsfc.nasa.gov/ssc/data/analysis/rmfit/>

Table 1. *Fermi*-LAT likelihood results for GRB 170214A.

$T_1 - T_2^a$ s	TS ^b	N_{ROI}^c	N_P^d	Γ_{LAT}^e	$F_L(0.1 - 10\text{GeV})^e$ $10^{-5}\text{ph cm}^{-2} \text{s}^{-1}$	$f_L(0.1 - 10\text{GeV})^e$ $10^{-8}\text{erg cm}^{-2} \text{s}^{-1}$
0 - 52	15	16	7.2	4.98 ± 2.62	3.01 ± 1.34	0.64 ± 0.34
52 - 62	11	4	4.0	6.96 ± 2.76	8.92 ± 4.44	1.71 ± 0.86
62 - 63	104	15	14.4	3.04 ± 0.54	285.06 ± 89.54	88.94 ± 29.37
63 - 64	308	16	16.0	4.05 ± 0.70	333.88 ± 182.45	79.51 ± 51.58
64 - 66	38	10	8.2	3.73 ± 0.91	84.86 ± 35.81	21.44 ± 9.35
66 - 67	20	5	5.0	3.93 ± 1.21	103.80 ± 46.62	25.21 ± 12.01
67 - 69	57	6	5.9	2.78 ± 0.73	57.75 ± 30.29	20.53 ± 11.44
69 - 70	19	5	3.7	3.19 ± 1.06	74.45 ± 40.72	21.82 ± 13.74
70 - 80	58	11	10.0	3.50 ± 0.79	20.37 ± 7.11	5.43 ± 2.26
80 - 90	196	11	11.0	2.50 ± 0.42	20.65 ± 6.29	8.95 ± 3.82
90 - 100	74	10	9.3	3.31 ± 0.70	18.65 ± 6.65	5.26 ± 2.07
100 - 110	58	6	5.2	1.54 ± 0.29	7.89 ± 3.79	11.89 ± 6.55
110 - 120	76	11	9.5	2.37 ± 0.43	16.90 ± 6.02	8.25 ± 3.96
120 - 130	92	12	11.1	2.01 ± 0.30	18.66 ± 6.11	13.81 ± 6.26
130 - 140	236	13	12.9	1.92 ± 0.25	21.39 ± 6.04	17.85 ± 7.34
140 - 150	97	16	13.0	2.20 ± 0.32	21.91 ± 6.38	12.75 ± 5.36
150 - 160	117	9	8.9	2.38 ± 0.44	15.35 ± 5.59	7.38 ± 3.63
160 - 170	108	7	7.0	2.35 ± 0.47	11.82 ± 4.51	5.88 ± 3.28
170 - 180	73	6	6.0	2.10 ± 0.43	9.37 ± 3.88	6.14 ± 3.79
180 - 190	147	8	8.0	2.27 ± 0.42	12.86 ± 4.60	6.91 ± 3.65
190 - 200	54	6	6.0	2.60 ± 0.60	9.89 ± 4.07	3.95 ± 2.22
200 - 300	142	43	39.7	2.67 ± 0.27	6.43 ± 1.17	2.45 ± 0.56
300 - 500	140	55	33.5	2.24 ± 0.21	2.58 ± 0.49	1.43 ± 0.38
500 - 700	65	38	20.8	2.50 ± 0.32	1.64 ± 0.41	0.71 ± 0.23
700 - 900	22	19	7.7	2.21 ± 0.43	0.59 ± 0.25	0.34 ± 0.20
190 - 900	380	161	106.2	2.44 ± 0.14	2.37 ± 0.54	1.07 ± 0.36

^aThe start analysis time (T_1) and the end analysis time (T_2) in unit of seconds.^bTS is the test-statistic value, which is roughly equal to σ^2 , where σ is the significance of GRB detection.^cThe observed LAT counts number within the region of interest (ROI), i.e., 12 degrees of GRB center position.^dThe predicted LAT counts number from GRB 170214A.^ePhoton index (Γ_{LAT}), photon flux (F_L) and energy flux (f_L) of GRB 170214A.

FV) component in GBM energy bands³. The Band function is employed as the photon spectrum model in each time bin, which is described by [Band et al. \(1993\)](#):

$$N(E) = A \begin{cases} (E/100\text{keV})^\alpha e^{(-E(2+\alpha)/E_p)} & \text{if } E < E_b \\ [(\alpha - \beta)E_p/(100\text{keV}(2 + \alpha))]^{(\alpha - \beta)} e^{\beta - \alpha} (-E/100\text{keV})^\beta & \text{if } E \geq E_b \end{cases}$$

where A is the normalization, $E_b = (\alpha - \beta)E_p/(2 + \alpha)$, α is the photon index at low energy, β is the photon index at high energy and E_p is the peak energy in the $E^2N(E)$ representation. The energy fluxes (f_G) are obtained between 10 keV and 10 MeV, as shown in Tab. 2.

For GRB 170214A, we build the light curves in two narrow energy bands, i.e., 8-200 keV and 200 keV-1 MeV. We employ a single power-law function (PL), i.e., $N(E) = N_0(E/100\text{keV})^{-\alpha_{\text{PL}}}$ (α_{PL} , the PL decay index), to model the photon spectrum

³ We are actually unable to recognize every single pulse with very short time variability in the light curves of energy flux (e.g., ~ 100 ms). However, we can still search temporal correlation in a longer timescale. The light curves of both the LAT emission and GBM emission show structures with a fast-rising followed by a fast-decaying in the time interval 52-80 s and 90-160 s respectively (see next section), so we define these structures as fast variable (FV) components to search the correlation in two energy bands.

in the former energy band, because the derived peak energy in the whole GBM energy range (8 keV-10 MeV) is always larger than ~ 200 keV. A Band function is used to model the photon spectrum for the latter energy band. The GBM fluxes in these two energy bands of GRB 170214A are present in Tab. 2.

3. TEMPORAL AND SPECTRAL ANALYSIS OF GRB 170214A

3.1. Light curves

The light curves of GRB 170214A in LAT (0.1-10 GeV) and GBM (10 keV-10 MeV) bands are plotted in Fig. 1, which can be described with four phases.

1. *0-52 s*: The LAT emission is too weak to be subdivided in this period, while the GBM emission show a few pulse structures.
2. *52-80 s* (Period 1): One fast variable (FV) component is found at both the LAT and GBM bands with fast rising and fast decaying behaviors. We fit it with an empirical smooth broken power law function (SBPL):

$$f(t) = f_0 \left[\left(\frac{t}{t_p} \right)^{-\alpha_r s} + \left(\frac{t}{t_p} \right)^{-\alpha_d s} \right]^{-1/s} \quad (1)$$

where f_0 is the normalisation in unit of $\text{erg cm}^{-2} \text{s}^{-1}$, t_p is the peak time of the FV component, and the temporal indices of the rising part and the decaying part are α_r and α_d respectively. Here s determines the smoothness of the peak, which is fixed at 10 for the fast variable components, following the suggestions in Liang et al. (2008). For both the GBM and LAT bands, the value of α_r can not be constrained given only two flux points in the rising part, and hence we fix their values based on the connection of the two data points in the two energy bands respectively, i.e., $\alpha_r = 40$ in LAT band and $\alpha_r = 20$ in GBM band. As shown in Tab. 3, both light curves decay steeply, i.e., $\alpha_d = -24 \pm 14.5$ in LAT band and $\alpha_d = -8.5 \pm 0.4$ in GBM band. Although the error bar of α_d is quite large in the LAT band, the result clearly shows a quick flux drop after the peak. Such strong variabilities imply that they are mostly likely to be related with central engine of GRB 170214A. The peak times t_p in both energy bands are consistent with each other with uncertainties, which are around 61.8 seconds after GBM trigger.

3. *90-160 s* (Period 2): One FV component appears in either the light curve both in the GBM or LAT band. By fitting them with a SBPL function, α_r is found to be 3.0 ± 1.1 for the LAT emission and 10.3 ± 1.0 for the GBM emission, which are a bit too rapid for the external reverse shock model. This is also proved by the large decay indices (α_d) in both energy bands, which are -10.7 ± 7.4 and -28.9 ± 17.8 for LAT and GBM emission respectively, although the resultant error bars are quite large. The peak times in both energy bands are consistently around 139 seconds after GBM trigger.
4. *160-900 s* (Extended phase): No GBM emission is detected in this phase, which implies GRB 170214A enters the so called afterglow phase. The LAT light curve shows a power law decay with decay index (α_{LAT}) of -1.6 ± 0.2 . The LAT photon index (Γ_{LAT}) in the time interval (190-900 s) is found to be -2.4 ± 0.1 , translating to a spectral index $\beta_{\text{LAT}} = \Gamma_{\text{LAT}} + 1 = -1.4 \pm 0.1$. In the external shock model, we have the synchrotron flux at high energy $f_{\text{LAT}} \propto \nu^\beta t^\alpha$. Considering that the LAT energy band (> 100 MeV) is usually above the external synchrotron cooling energy ($h\nu_c$, h is the plank constant), we can derive the injection electron spectrum power index p to be ~ 2.8 from $f_{\text{LAT}} \propto \nu^{-p/2}$. This predicts a power-law index of about -1.6 for the light curve in the external shock model, i.e., $f_{\text{LAT}} \propto t^{(2-3p)/4}$ (Sari et al. 1998), which is consistent with the observed one, that is -1.6 ± 0.2 . Thus, we conclude that the late LAT emission can be well explained by the external shock model.

Second, we perform a global fit to the LAT light curve in the whole detection interval, i.e., 0-900 seconds. Based on above analysis, we decompose three components from the LAT light curve, i.e., the Period 1, Period 2 and an underlying component, Period 3, with each of them modeled by a SPBL. The results are present in Tab. 3 and plotted in Fig. 1. As for the Period 1 and Period 2, the results are similar to that discussed above. For the Period 3 (with sharpness s of 3), the peak time is around 145 s, which can be explained as the dynamic deceleration time of the ejecta. The rising temporal index is around 2.1, which is consistent with the expected index (~ 2.0) in the external shock model (Kumar & Barniol Duran 2009; Ghisellini et al. 2010). Apparently, the flux of the Period 3 is comparable with that of the Period 2 at ~ 160.8 seconds after GBM trigger, after which the afterglow emission takes over. This time is also consistent with the end time of GBM emission.

3.2. Spectral analysis

In the Period 1 and Period 2, we perform a joint spectral fit employing the GBM and LAT data between 8 keV and 10 GeV. The Castor Statistic (CSTAT) is used in the spectral fit, as in other bright LAT GRBs (Abdo et al. 2009b; Ackermann et al. 2010,

Table 2. *Fermi*-GBM results for GRB 170214A.

$T_1 - T_2^a$ s	$f_G(10\text{keV} - 10\text{MeV})^b$ $10^{-7}\text{erg cm}^{-2} \text{ s}^{-1}$	$f_G(200\text{keV} - 1\text{MeV})^b$ $10^{-7}\text{erg cm}^{-2} \text{ s}^{-1}$	$f_G(8\text{keV} - 200\text{MeV})^b$ $10^{-7}\text{erg cm}^{-2} \text{ s}^{-1}$
0 - 2	8.23 ± 1.60	3.78 ± 0.61	1.73 ± 0.13
2 - 4	14.70 ± 3.79	3.69 ± 0.84	2.27 ± 0.14
4 - 6	21.40 ± 4.43	3.89 ± 0.12	2.99 ± 0.15
6 - 8	18.80 ± 4.80	7.92 ± 0.77	3.31 ± 0.15
8 - 10	27.60 ± 5.01	10.20 ± 0.75	4.10 ± 0.15
10 - 12	23.80 ± 4.99	9.41 ± 0.73	4.18 ± 0.15
12 - 14	29.40 ± 4.82	12.60 ± 0.82	5.77 ± 0.17
14 - 16	27.40 ± 1.81	12.10 ± 0.72	5.67 ± 0.16
16 - 18	35.40 ± 5.14	16.00 ± 2.68	6.95 ± 0.17
18 - 20	37.00 ± 1.76	16.50 ± 0.82	6.81 ± 0.18
20 - 22	41.40 ± 5.00	18.40 ± 0.84	8.06 ± 0.18
22 - 24	27.10 ± 4.62	12.40 ± 0.77	7.02 ± 0.17
24 - 26	16.40 ± 0.92	7.25 ± 0.67	5.32 ± 0.15
26 - 28	16.30 ± 1.44	<10.3	4.36 ± 0.15
28 - 30	20.50 ± 4.00	10.10 ± 0.71	6.69 ± 0.16
30 - 32	24.30 ± 4.26	8.00 ± 0.70	5.48 ± 0.16
32 - 34	20.80 ± 4.21	9.37 ± 0.70	6.24 ± 0.16
34 - 36	38.00 ± 2.01	16.30 ± 0.85	6.75 ± 0.17
36 - 38	39.00 ± 4.92	20.00 ± 0.89	8.85 ± 0.18
38 - 40	39.60 ± 1.87	16.80 ± 1.37	8.35 ± 0.17
40 - 42	39.80 ± 1.88	17.80 ± 0.97	7.08 ± 0.18
42 - 44	55.00 ± 5.00	25.00 ± 0.93	9.89 ± 0.19
44 - 46	68.70 ± 5.41	26.50 ± 2.87	9.58 ± 0.20
46 - 48	54.00 ± 5.15	19.20 ± 1.02	7.73 ± 0.19
48 - 50	47.50 ± 2.04	20.30 ± 1.13	8.28 ± 0.18
50 - 52	68.40 ± 4.10	23.80 ± 0.90	9.72 ± 0.20
52 - 62	39.00 ± 1.89	15.60 ± 0.34	7.66 ± 0.08
62 - 63	133.00 ± 6.13	33.70 ± 1.51	12.10 ± 0.29
63 - 64	98.10 ± 5.99	27.90 ± 1.70	9.93 ± 0.27
64 - 66	59.80 ± 3.90	20.60 ± 0.83	9.55 ± 0.19
66 - 67	56.20 ± 5.78	19.10 ± 1.25	8.86 ± 0.25
67 - 69	47.00 ± 3.84	14.90 ± 0.81	7.91 ± 0.18
69 - 70	29.40 ± 4.42	<16.7	5.01 ± 0.21
70 - 80	28.90 ± 1.82	12.70 ± 0.60	7.19 ± 0.08
80 - 90	7.02 ± 1.58	<5.1	2.16 ± 0.06
90 - 100	2.74 ± 1.39	0.44 ± 0.25	1.24 ± 0.05
100 - 110	6.97 ± 1.25	1.83 ± 0.42	2.25 ± 0.06
110 - 120	4.44 ± 0.61	<2.2	0.90 ± 0.05
120 - 130	9.33 ± 1.36	1.71 ± 0.30	1.86 ± 0.06
130 - 140	22.80 ± 1.80	7.61 ± 0.32	5.65 ± 0.07
140 - 150	6.08 ± 1.11	<4.2	1.97 ± 0.06
150 - 160	2.16 ± 1.06	<1.2	0.24 ± 0.06

^aThe start analysis time (T_1) and the end analysis time (T_2) in unit of seconds.^bGBM energy flux in corresponding energy range.

Table 3. Temporal behaviors of GRB 170214A in LAT and GBM band.

$T_1 - T_2$ s	Period	LAT				GBM			
		α_r^a	α_d^a	t_p^a s	s^a	α_r^a	α_d^a	t_p^a s	s^a
52 - 80	1	40 (fixed)	-24 ± 14.5	62.3 ± 1.1	10	20 (fixed)	-8.5 ± 0.4	60.7 ± 0.4	10
90 - 160	2	3.0 ± 1.1	-10.7 ± 7.4	140.5 ± 14.9	10	10.3 ± 1.0	-28.9 ± 17.8	137.8 ± 3.4	10
0 - 900	3	2.1 ± 0.4	-1.6 ± 0.2	145 ± 21.9	3	-	-	-	-

^aThe parameters of smoothly broken power-law function (SBPL), α_r is the rising index before the peak time of t_p , after which the temporal decay index is α_d , s is the smoothness of the break.

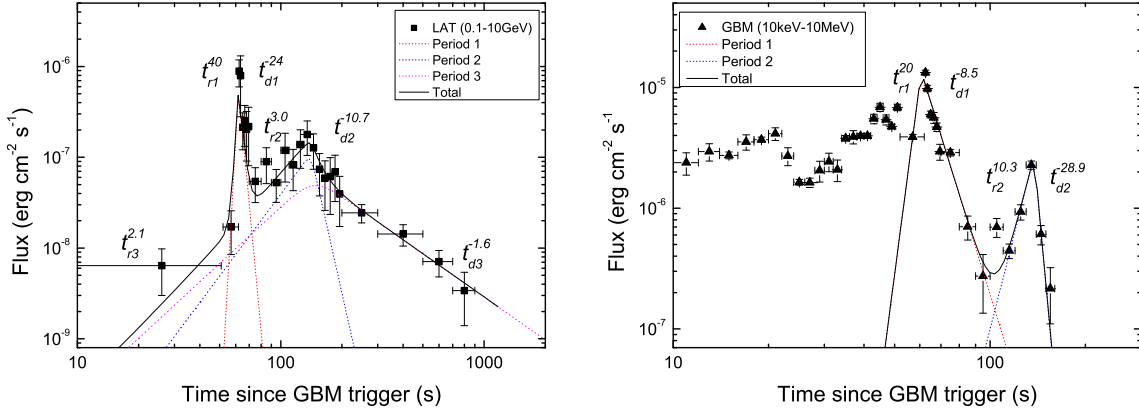


Figure 1. The LAT and GBM light curves of GRB 170214A with the best fits to these data. The rising and decay indices (α_r and α_d) for each component are labeled in corresponding position.

2011). For the same degrees of freedom (DOF), the smaller the CSTAT value is, the better the photon model is for the data. The results are present in Tab. 4, where the photon index Γ_{LAT} that derived from the LAT data only is also presented to compare with results of the GBM+LAT joint fit. The results are also shown in Fig. 2.

For the intensive period of 52-80 s, the Band parameters, α , β and E_p , are found to be -0.74 ± 0.02 , -2.34 ± 0.06 and 361 ± 12 keV respectively. The CSTAT value is 600 with DOF of 348. Γ_{LAT} from the LAT data only is much softer than β from the GBM+LAT joint fit in this period, i.e., $-\Gamma_{\text{LAT}}$ of -3.49 ± 0.28 comparing with β of -2.34 ± 0.06 . Thus, we test a BandCut model, which is described as the Band with a high energy cutoff, i.e., e^{-E/E_c} , where E_c is the exponential cutoff energy. With one more parameter, the BandCut will be regarded as a more preferred model than a single Band if $\Delta(\text{CSTAT})$ is larger than 28 (Ackermann et al. 2013; Tang et al. 2015). However, only $\Delta(\text{CSTAT}) \sim 25$ is found for the BandCut model with a cutoff energy of 224 ± 58 MeV. Therefore, we consider they are the equally good models in this period. Alternatively, when a power law function is added to the Band model, i.e., Band+PL, the fit becomes even worse than a single Band with a larger CSTAT value.

For the second period of 90-160 s, α , β and E_p in the Band model are -1.30 ± 0.03 , -2.25 ± 0.11 and 292 ± 37 keV respectively, with the CSTAT/DOF of 714/348. The photon index of the LAT data is 2.12 ± 0.13 , which is consistent with the high-energy photon index β of the GBM+LAT joint fit. The spectrum fit in this period cannot be improved significantly by either employing another fitting function or adding an additional component to the Band function, i.e., with a larger CSTAT value.

The result implies the prompt GBM emission and the prompt LAT emission of GRB 170214A may come from the same region, and disfavors the existence of other spectral components in these two periods.

3.3. KeV/MeV-GeV correlation and the variability of LAT FV component

3.3.1. method

First, the keV/MeV-GeV correlation between the GBM energy flux (f_L) and LAT energy flux (f_G) is tested in a certain time period from T_1 to T_2 with several time bins, i.e., N_{bin} . Assuming $f_L(T_i)$ and $f_G(T_i)$ are the LAT flux and GBM flux at the time of T_i , the linear equation can be represent as:

$$f_L(T_i) = A + B \times f_G(T_i) \quad (2)$$

Table 4. Spectral analysis results of GRB 170214A in two periods.

	GBM+LAT 8keV-10 GeV						LAT 0.1-10 GeV
$T_1 - T_2$ s	Model ^a	α^a	β^a	E_p^a keV	E_c^b MeV	CSTAT/DOF ^c	Γ_{LAT}^d
52 - 80	Band	-0.74 ± 0.02	-2.34 ± 0.06	361 ± 12	-	600/348	3.49 ± 0.28
...	BandCut	-0.73 ± 0.01	-2.25 ± 0.02	355 ± 6	224 ± 58	575/347	...
90 - 160	Band	-1.30 ± 0.03	-2.25 ± 0.11	292 ± 37	-	714/348	2.12 ± 0.13

^aThe spectral parameters of Band model, α is the photon index below the peak energy of E_p , above which the photon index is β .

^bThe high-energy exponential cutoff energy.

^cThe Castor Statistic (CSTAT) value and the degree of freedom (DOF).

^dPhoton index of the LAT data only.

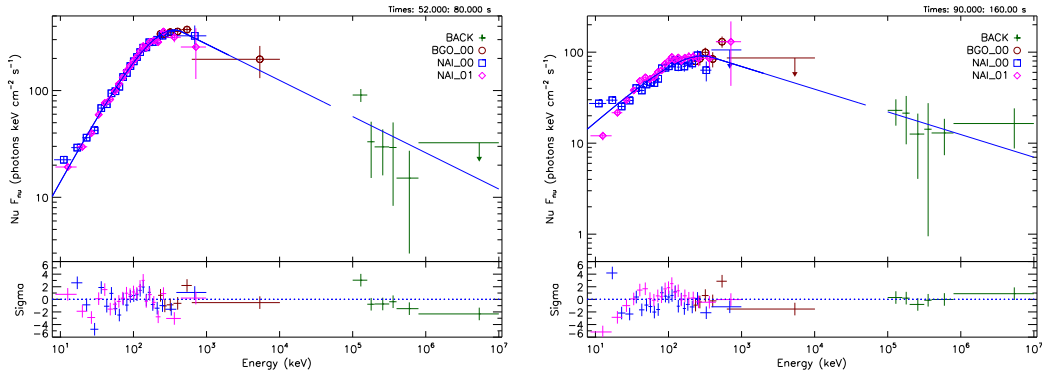


Figure 2. The GBM+LAT joint energy spectrum fits of GRB 170214A in two periods, which are modeled as the “Band” function (Band et al. 1993). For the former, $\alpha = -0.74 \pm 0.02$, $\beta = -2.34 \pm 0.06$ and $E_p = 361 \pm 12$ keV, and for the latter, $\alpha = -1.30 \pm 0.03$, $\beta = -2.25 \pm 0.11$ and $E_p = 292 \pm 37$ keV.

According to Pearson’s correlation coefficient R can be represent:

$$R = \frac{\sum_1^{N_{\text{bin}}} (f_G(T_i) - \bar{f}_G)(f_L(T_i) - \bar{f}_L)}{\sqrt{\sum_1^{N_{\text{bin}}} (f_G(T_i) - \bar{f}_G)^2} \sqrt{\sum_1^{N_{\text{bin}}} (f_L(T_i) - \bar{f}_L)^2}} \quad (3)$$

where the \bar{f}_L and \bar{f}_G represent respectively the average fluxes of the LAT band and the GBM band in the chosen time interval. We also calculate the p value of the null hypothesis using the software of *Origin*, which can be described as the confidence level of $1 - p$ for the keV/MeV-GeV correlation. A strong correlation can be claimed when $R > 0.8$ while a moderate correlation can be claimed when $0.5 < R < 0.8$ (Newton & Rudestam 1999). In above two cases, the p value should be smaller than 0.05, which represents a 95% confidence level of the correlation. Since the R value in each fit is larger than 0 ($R = 0$, no correlation) in our analysis, thus other cases are defined as a weak correlation. We first test the correlation in the whole prompt emission duration, which covers the time period of both GBM and LAT detection (labeled as “Trace” hereafter). Second, we try to determine whether the correlation exists in some sub periods, such as in the FV components.

Second, the ratio \mathcal{L} is calculated between the duration of the full width at half-maximum (FWHM) of the SBPL-fit result and the whole duration of the FV component. The FWHM duration ω is derived by time spanning a half of the SBPL peak flux in the LAT light curve. The period T ($=T_2 - T_1$) is the lower-limit value of the duration of the FV component, which often lasts a longer duration than T as shown in Fig .1 and Fig .4. We regard it as a rapid variability of the LAT FV component if (1) the post-peak decay index α_d being sharper than -3.0 , since such a sharp decay index cannot be explained by external forward shocks (Kobayashi & Zhang 2003; Burrows et al. 2005), and (2) the ratio \mathcal{L} being smaller than 1.0 significantly, which implies a rapid variability timescale (Ackermann et al. 2011).

3.3.2. Result

First, we test the correlation between the LAT (0.1-10 GeV) and GBM (10 keV-10 MeV) light curves during the prompt phase. In the Trace period, R is 0.90 with $p < 10^{-4}$, which implies a strong correlation between the GBM and LAT emission. In both

the Period 1 and Period 2, the strong correlations are also found with R of 0.95 and 0.82 respectively, as shown in Tab. 5.

Second, the correlations of the LAT emission (0.1-10 GeV) and two sub energy bands of GBM emission, i.e., 8-200 keV and 200 keV-1 MeV, are tested. For the case of 8-200 keV, the LAT-detected emission correlates with that detected in GBM band moderately in the Trace period while in the Period 1 and Period 2, they show a moderate and strong correlation respectively, which can be found in Tab. 5. As for 200 keV-1 MeV, strong correlations between the emission in the LAT and GBM energy band are found in both the Trace period and the Period 1. However, a weak correlation, with p value of 0.17 is found in the Period 2 due to non-detection of the 200 keV-1 MeV emission in four time bins of this period.

Third, we study the GeV variability of the two LAT FV components during the Period 1 and Period 2, the results of which are given in Tab. 6. For the first FV component with α_d of -23.88 ± 14.5 and $\mathcal{L} < 0.09$, it exhibits a rapid variability. For the second FV component, we find it is a rapid variability with α_d of -10.66 ± 7.36 and $\mathcal{L} < 0.60$, although with a large uncertainty on the decay power-law index.

The above results on the temporal correlation of keV/MeV-GeV and the temporal variability of the LAT FV components suggest that the prompt high-energy emission in GRB 170214A cannot be produced in the external shock region, but may share the same internal origin as the GBM emission.

4. CASE FOR OTHER BRIGHT LAT GRBS

In this section, we study the keV/MeV-GeV correlation and the variability of the possible LAT FV components for other five bright LAT GRBs, i.e., GRB 080916C, GRB 090510, GRB 090902B, GRB 090926A and GRB 130427A. The results are shown in Tab. 5, Fig. 3, Tab. 6 and Fig. 4.

4.1. GRB 080916C

In the Trace period, the GBM and LAT light curves show a moderate correlation with R of 0.59 and p of 0.0026.

We search the GeV variability in the first 10 seconds, i.e., between 3.7 – 9.7 s. The GeV emission with $\alpha_d = -5.38 \pm 1.83$ and $\mathcal{L} < 0.22$ infers a rapid variability in this period. The resultant peak time of 5.9 ± 0.2 is consistent the prominent peak in the time interval of 3.6 – 7.7 s (Abdo et al. 2009a).

4.2. GRB 090510

GRB 090510 is a short GRB. We find that there is a weak correlation in the Trace period, i.e., 0.3 – 0.9 s.

The emission in the LAT band show a rapid rising in the Trace period, after which it exhibits a fast decaying. Thus we extended the time interval to a longer period as a possible FV component, i.e., 0.3 – 1.5 s. In this time interval, the LAT light curve shows a rapid variability with $\alpha_d = -4.49 \pm 0.39$ and $\mathcal{L} < 0.17$. The discrepancy between the peak times in the GBM and the LAT light curve is about 0.15 seconds, which is comparable with the time lag between the GBM and LAT light curves derived in Ackermann et al. (2010), i.e., 0.25 ± 0.05 s.

4.3. GRB 090902B

Moderate correlations are found between the GBM and LAT light curves in the Trace period, Period 1 (0 – 12.5 s) and Period 2 (12.5 – 23 s).

The LAT light curve is subdivided into two possible FV components for variability analysis, i.e., 0 – 12.5 s and 12.5 – 23 s, which is same as the Period 1 and Period 2. For the first FV component, the variability is rapid with $\alpha_d = -7.23 \pm 3.60$ and $\mathcal{L} < 0.30$. The peak time of the first FV components (10.3 ± 0.4 s) is consistent with that discovered in Abdo et al. (2009b), which is around 9 s. For the second FV component, the resultant α_d with a large uncertainty, i.e., $\alpha_d = -3.24 \pm 1.73$, and $\mathcal{L} < 0.53$ can be a rapid variability.

4.4. GRB 090926A

A weak correlation is found between the GBM and LAT light curves in the Trace period, although both the light curves show the rapid variabilities. However, we find a strong correlation in the first 8.5 seconds, with R of 0.89.

The LAT light curve indeed shows a fast variability. Thus two possible FV components are employed to search the GeV variability, i.e., 2 – 8.5 s and 8.5 – 16.5 s. For the first FV component, the variability is rapid with α_d of -10.63 ± 4.25 and $\mathcal{L} < 0.26$. The peak time (7.0 ± 0.2 s) of the first FV component locates at the time interval “b” (3.3 – 9.8 s) (Ackermann et al. 2011). For the second FV component, we find the LAT light curve could be decomposed into sub structures. Three SBPL components are employed to fit the GeV light curve, the results can be shown in Tab. 6. All of them exhibit the rapid variabilities with α_d much sharper than -3 and $\mathcal{L} < 0.39$. One of the peak times, i.e., 9.9 ± 0.2 s, is consistent with the peak time in the time interval “c” (9.8 – 10.5 s) in Ackermann et al. (2011).

Table 5. Correlation analysis results of GRB 170214A and other five bright LAT GRBs.

GRB Name	GBM($E_1 - E_2$) keV	LAT($E_1 - E_2$) GeV	$T_1 - T_2$ s	Period	N_{bin}	R	p	Correlation ^a
170214A	10 - 10000	0.1 - 10	52 - 160	Trace	16	0.90	$< 10^{-4}$	Strong
...	52 - 80	1	8	0.95	3.7×10^{-3}	Strong
...	90 - 160	2	7	0.81	2.9×10^{-2}	Strong
...	8 - 200	...	52 - 160	Trace	16	0.68	4.0×10^{-3}	Moderate
...	52 - 80	1	8	0.75	3.3×10^{-2}	Moderate
...	90 - 160	2	7	0.85	1.5×10^{-2}	Strong
...	200 - 1000	...	52 - 160	Trace	11	0.81	2.7×10^{-3}	Strong
...	52 - 80	1	7	0.96	7.4×10^{-4}	Strong
...	90 - 160	2	4	0.83	0.17	Weak
080916C	10 - 10000	0.1 - 10	3.7 - 53.3	Trace	24	0.59	2.6×10^{-3}	Moderate
090510	10 - 10000	...	0.3 - 0.9	Trace	4	0.09	0.91	Weak
090902B	10 - 10000	...	0 - 23	Trace	27	0.73	$< 10^{-4}$	Moderate
...	0 - 12.5	1	13	0.76	2.6×10^{-3}	Moderate
...	12.5 - 23	2	14	0.53	4.6×10^{-2}	Moderate
090926A	10 - 10000	...	2 - 16.5	Trace	26	0.12	0.56	Weak
...	5.5 - 8.5	1	6	0.89	1.7×10^{-2}	Strong
130427A	10 - 10000	...	0 - 200	Trace	20	0.16	0.51	Weak

Note: (1) $R > 0.8$ for strong positive correlation ($p < 0.05$); (2) $0.5 < R < 0.8$ for moderate positive correlation ($p < 0.05$); (3) $0 < R < 0.5$ for weak positive correlation (Newton & Rudestam 1999).

4.5. GRB 130427A

In the Trace period, the correlation between the LAT-detected and GBM-detected emissions is weak. This is consistent with the conclusion drawn by Ackermann et al. (2014), i.e., the LAT-detected emission does not appear to be temporally correlated with the GBM emission beyond the initial spike at GBM trigger.

We then perform the analysis in the first 70 seconds of the LAT-detected emission, a possible FV component, to study the GeV variability. $\alpha_d = 1.71 \pm 0.24$ implies that the variability is not rapid enough to support an internal origin in this period.

5. CONCLUSION

In this work, we performed the temporal and spectral analysis on GRB 170214A, which shown that the LAT and GBM emission may share the same origin. We thus presented a quantitative analysis of the temporal correlation between the prompt keV/MeV and high-energy ($> 100\text{MeV}$) emission of GRB 170214A. Given the strong correlation found in the periods of the fast variable components and the Trace period, we suggested that the prompt high-energy and keV/MeV emission of GRB 170214A may arise from the same process, say, certain internal dissipation process. Such a temporal correlation is also found in some other LAT GRBs, i.e., GRB 080916C, 090902B and 090926A. The rapid temporal variability found in LAT emission further supports the internal origin of the high-energy emission in these four GRBs as well as GRB 090510. As our work only deals with the prompt high-energy emission in several bright LAT GRBs, we need more LAT GRBs with high quality data in future to check whether this is a general case for all the GRBs.

We thank the anonymous referee for constructive comments, which helped us to improve the manuscript. We are grateful for John F. Beacom and Bei Zhou for a helpful revision of this manuscript. T.Q.W. is supported by the Natural Science Foundation of China under grants No. 11547029, 11533004, the Youth Foundation of Jiangxi Province (No. 20161BAB211007), the Postdoctoral Foundation of Jiangxi Province (No. 2016KY17), the Natural Science Foundation of Jiangxi Provincial Department of Education (No. GJJ150077). W.X.Y. is supported by the 973 program under grant 2014CB845800, the NSFC under grants 11625312 and 11033002.

Facility: Fermi

REFERENCES

- Abdo, A. A., Ackermann, M., Arimoto, M., et al. 2009a, *Science*, 323, 1688
- Abdo, A. A., Ackermann, M., Ajello, M., et al. 2009b, *ApJL*, 706, L138

Table 6. GeV variability of the possible FV components in other five LAT GRBs.

GRB ^a	$T_1 - T_2$ s	α_r^b s	α_d^b	t_p^b	s^b	ω^c	\mathcal{L}^d	Variability ^e
170214A_1	52 - 80	40.00 (fixed)	-23.88 ± 14.5	62.3 ± 1.1	10	2.4 ± 0.5	< 0.09	Y
170214A_2	90 - 160	2.96 ± 1.06	-10.66 ± 7.36	140.5 ± 14.9	10	41.8 ± 7.0	< 0.60	Y
080916C	3.7 - 9.7	10.00 ± 3.85	-5.38 ± 1.83	5.9 ± 0.2	10	1.3 ± 0.2	< 0.22	Y
090510	0.3 - 1.5	14.55 ± 4.91	-4.49 ± 0.39	0.8 ± 0.02	10	0.2 ± 0.02	< 0.17	Y
090902B_1	0 - 12.5	2.47 ± 0.84	-7.23 ± 3.60	10.3 ± 0.4	10	3.8 ± 0.5	< 0.30	Y
090902B_2	12.5 - 23	5.62 ± 2.56	-3.24 ± 1.73	15.9 ± 0.6	10	5.6 ± 0.9	< 0.53	Y
090926A_1	2 - 8.5	4.04 ± 0.92	-10.63 ± 4.25	7.0 ± 0.2	10	1.7 ± 0.3	< 0.26	Y
090926A_2a	8.5 - 11.5	19.47 ± 7.61	-13.32 ± 5.07	9.9 ± 0.2	10	0.9 ± 0.07	< 0.31	Y
090926A_2b	11.5 - 13.5	72 (fixed)	-29.08 ± 11.53	11.9 ± 0.2	10	0.4 ± 0.05	< 0.22	Y
090926A_2c	13.5 - 16.5	25.17 ± 4.89	-14.99 ± 4.78	14.5 ± 0.1	10	1.2 ± 0.1	< 0.39	Y
130427A	0 - 70	1.10 ± 0.18	-1.71 ± 0.24	20.5 ± 1.5	3	23.0 ± 1.8	< 0.33	N

^aThe subscript represents the index of the FV component.^bThe parameters of smoothly broken power-law function (SBPL), α_r is the rising index below the peak time of t_p , above which the decay index is α_d , s is the smoothness of the break.^cDuration of the full width at half-maximum in the light curve of the FV component.^dRatio between ω and $T(=T_2 - T_1)$.^eA rapid variability when the central value of α_d is smaller than -3 and $\mathcal{L} < 1.0$.

- Ackermann, M., Ajello, M., Asano, K., et al. 2011, *ApJ*, 729, 114
Ackermann, M., Asano, K., Atwood, W. B., et al. 2010, *ApJ*, 716, 1178
Ackermann, M., Ajello, M., Asano, K., et al. 2013, *ApJS*, 209, 11
Ackermann, M., Ajello, M., Asano, K., et al. 2014, *Science*, 343, 42
Band, D., Matteson, J., Ford, L., et al. 1993, *ApJ*, 413, 281
Beardmore, A. P., D'Ai, A., Melandri, A., et al. 2017a, GRB Coordinates Network, 20691, 1
Beardmore, A. P., D'Ai, A., Melandri, A., et al. 2017b, GRB Coordinates Network, 20679, 1
Beloborodov, A. M., Hascoët, R., & Vurm, I. 2014, *ApJ*, 788, 36
Burrows, D. N., Romano, P., Falcone, A., et al. 2005, *Science*, 309, 1833
Corsi, A., Guetta, D., & Piro, L. 2010, *ApJ*, 720, 1008
De Pasquale, M., Schady, P., Kuin, N. P. M., et al. 2010, *ApJL*, 709, L146
Frederiks, D., Golenetskii, S., Aptekar, R., et al. 2017, GRB Coordinates Network, 20678, 1
Ghirlanda, G., Ghisellini, G., & Nava, L. 2010, *A&A*, 510, L7
Gao, W.-H., Mao, J., Xu, D., & Fan, Y.-Z. 2009, *ApJL*, 706, L33
Ghisellini, G., Ghirlanda, G., Nava, L., & Celotti, A. 2010, *MNRAS*, 403, 926
Kobayashi, S., & Zhang, B. 2003, *ApJ*, 597, 455
Kruehler, T., Schady, P., Greiner, J., & Tanvir, N. R. 2017, GRB Coordinates Network, 20686, 1
Kumar, P., & Barniol Duran, R. 2009, *MNRAS*, 400, L75
Kumar, P., & Barniol Duran, R. 2010, *MNRAS*, 409, 226
Liang, E.-W., Racusin, J. L., Zhang, B., Zhang, B.-B., & Burrows, D. N. 2008, *ApJ*, 675, 528-552
Mailyan, B., & Meegan, C. 2017, GRB Coordinates Network, 20675, 1
Malesani, D., Krogager, J.-K., & Ranjan, A. 2017, GRB Coordinates Network, 20683, 1
Mattox, J. R., Bertsch, D. L., Chiang, J., et al. 1996, *ApJ*, 461, 396
Mazaeva, E., Pozanenko, A., Klunko, E., & Volnova, A. 2017, GRB Coordinates Network, 20687, 1
Newton, R. R., Rudestam, K. E. 1999, *Your Statistical Consultant: Answers to your Data Analysis Questions*. Thousand Oaks, CA: Sage Publications
Racusin, J. L., Vianello, G., & Perkins, J. 2017, GRB Coordinates Network, 20676, 1
Razzaque, S. 2010, *ApJL*, 724, L109
Sari, R., Piran, T., & Narayan, R. 1998, *ApJL*, 497, L17
Schady, P., Greiner, J., Steinmassl, S. 2017a, GRB Coordinates Network, 20680, 1
Schady, P., & Kruehler, T. 2017, GRB Coordinates Network, 20684, 1
Tang, Q.-W., Peng, F.-K., Wang, X.-Y., & Tam, P.-H. T. 2015, *ApJ*, 806, 194
Troja, E., Butler, N., Watson, A., et al. 2017a, GRB Coordinates Network, 20681, 1
Troja, E., Butler, N., Watson, A., et al. 2017b, GRB Coordinates Network, 20685, 1
Wang, X.-Y., He, H.-N., Li, Z., Wu, X.-F., & Dai, Z.-G. 2010, *ApJ*, 712, 1232
Zhang, B.-B., Zhang, B., Liang, E.-W., et al. 2011, *ApJ*, 730, 141

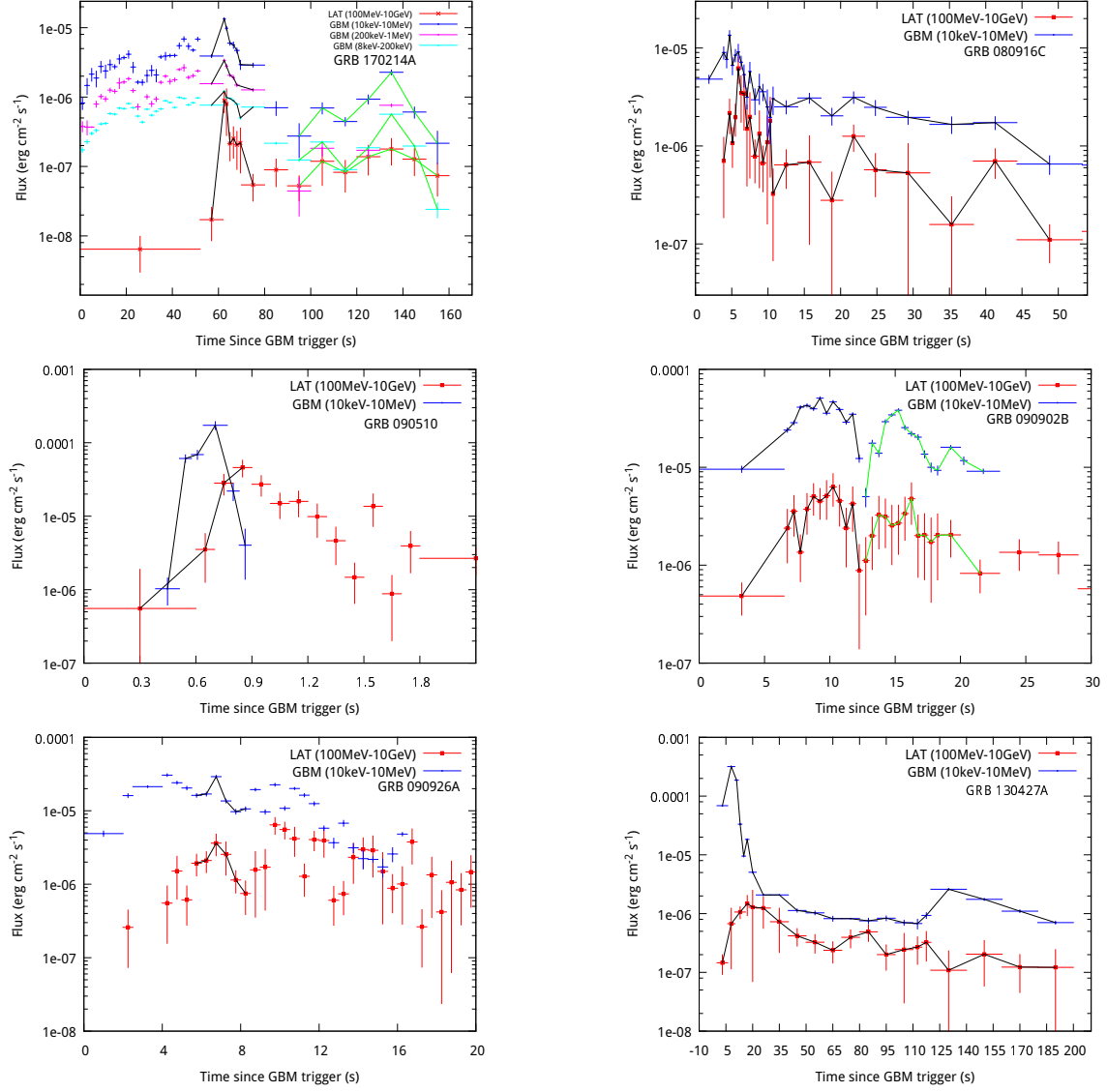


Figure 3. keV/MeV-GeV correlation. (1) GRB 170214A: strong for the Trace period, Period 1 (black line) and Period 2 (green line); (2) GRB 080916C: moderate for the Trace period; (3) GRB 090510: weak for the Trace period; (4) GRB 090902B: moderate for the Trace period, Period 1 (black line) and Period 2 (green line); (5) GRB 090926A: weak for the Trace period, strong for the Period 1 (black line); (6) GRB 130427A: weak for the Trace period.

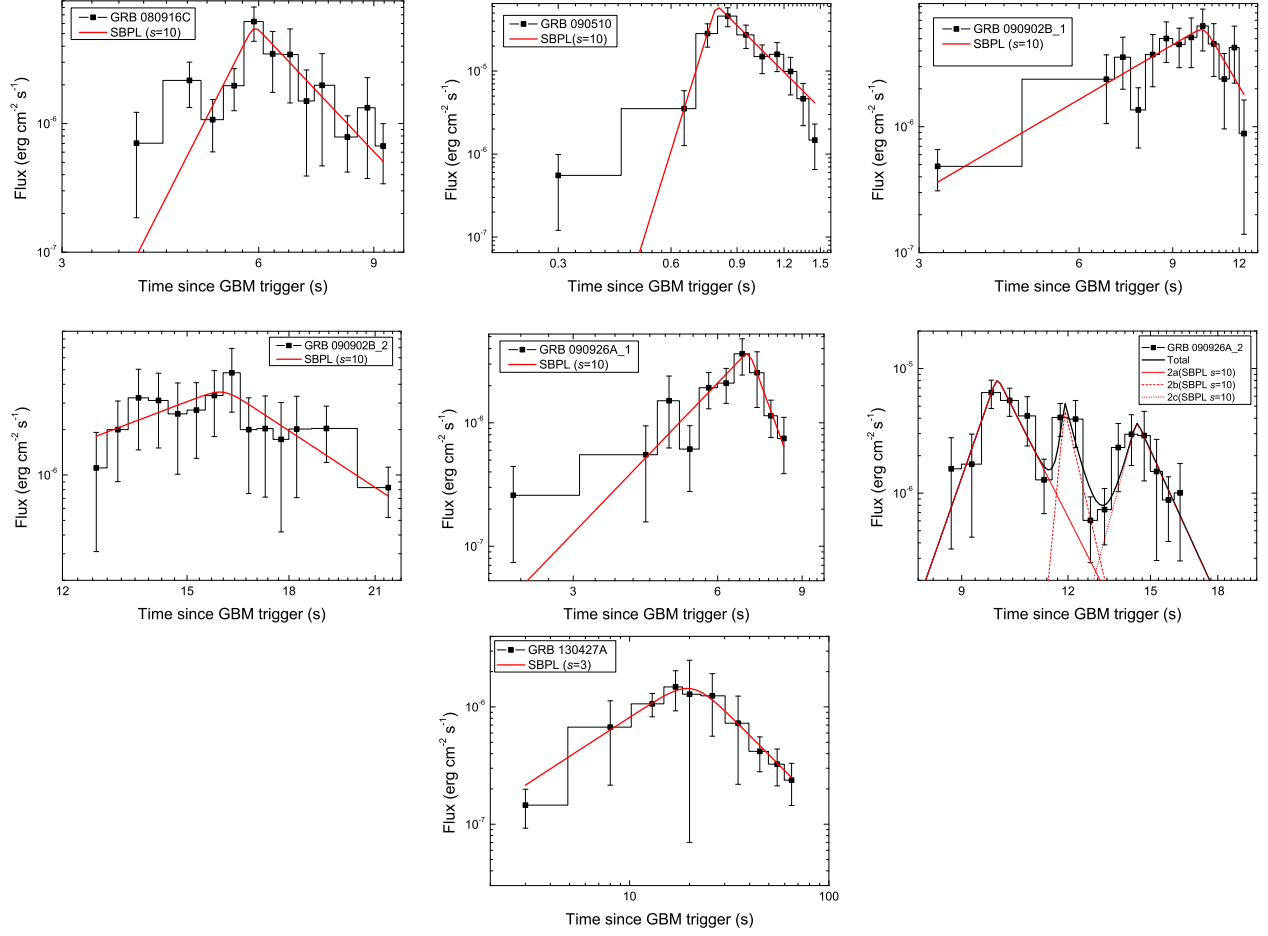


Figure 4. GeV variability analysis for the possible FV components in other five bright LAT GRBs. The filled-square represent the LAT data. The solid line is the best SBPL result of each GRB. For the second FV component of GRB 090926A, three sub structures are found, which are labeled as “2a”, “2b”, “2c” respectively. The s value is the corresponding smoothness for the SBPL function.